

Statistical fission parameters for nuclei at high excitation and angular momenta

M. Blann and T. T. Komoto

E Division, Lawrence Livermore National Laboratory, Livermore, California 94550

(Received 25 January 1982)

Experimental fusion/fission excitation functions are analyzed by the statistical model with modified rotating liquid drop model barriers and with single particle level densities modeled for deformation for ground state (a_v) and saddle point nuclei (a_f). Values are estimated for the errors in rotating liquid drop model barriers for the different systems analyzed. These results are found to correlate well with the trends predicted by the finite range model of Krappe, Nix, and Sierk, although the discrepancies seem to be approximately 1 MeV greater than the finite range model predictions over the limited range tested. The *a priori* values calculated for a_f and a_v are within $\pm 2\%$ of optimum free parameter values. Analyses for barrier decrements explore the importance of collective enhancement on level densities and of nuclear deformation in calculating transmission coefficients. A calculation is performed for the ^{97}Rh nucleus for which a first order angular momentum scaling is used for the $J=0$ finite range corrections. An excellent fit is found for the fission excitation function in this approach. Results are compared in which rotating liquid drop model barriers are decremented by a constant energy, or alternatively multiplied by a constant factor. Either parametrization is shown to be capable of satisfactorily reproducing the data although their $J=0$ extrapolated values differ markedly from one another. This underscores the dangers inherent in arbitrary barrier extrapolations.

NUCLEAR REACTIONS Deduced corrections to rotating liquid drop model barriers for selected data sets via statistical model fitting. Considered uncertainties due to collective enhancement of level densities, deformation effects on transmission coefficients. Compared deduced corrections to predictions of the finite range model.

I. INTRODUCTION

The present work is an attempt to deduce physically significant statistical fission parameters (angular momentum dependent fission barriers and single particle ratios) from experimental heavy ion induced fusion/fission excitation functions. The parameters involved are the angular momentum dependent fission barriers, $B_f(J)$, and the average single particle level density ratios a_f/a_v at saddle and ground state deformations.

Fitting of experimental fusion/fission excitation functions via statistical fission/evaporation codes has been done in the past.¹⁻⁶ Results yielded convenient parametrizations of the data; however, most authors recognized that all sins of omission in the analyses were forced into the extracted parameters, rendering their physical interpretation at best questionable. Unfortunately there has also been some temptation, not only to accept these parameters

literally, but to extrapolate them arbitrarily from the range of angular momenta in which they are determined to the zero angular momentum region.

In the present investigation we will explore questions such as the influence on parameters extracted due to collective enhancement of level densities, the modeling of transmission coefficients for deformed nuclei, and the range of a_f/a_v values permitted by the data. The uncertainties due to these effects will be converted into plus or minus uncertainties in the angular momentum dependent barrier parametrizations. These results for a variety of target-projectile systems will then be compared with the available theoretical guideposts: the rotating liquid drop model (RLDM) (Ref. 7) and the predicted finite range (FR) correction to liquid drop model barriers.^{8,9}

In Sec. II, we review previous work on the RLD and FR models relating to angular momentum dependent fission barriers. Several examples are

shown and a few different methods of modifying these barriers are illustrated. A suggestion for first order scaling of the $J=0$ FR correction to nonzero angular momenta is presented. In Sec. III, the different level density prescriptions used in the data analyses are presented and compared, and the model used to calculate a_f and a_v is described. Section IV contains comparisons of calculated and experimental excitation functions, where barrier parameters and parametrizations are varied.

From these calculations, corrections to the RLDM barriers and their uncertainties are estimated. In Sec. V these results are compared with predictions of the FR model. Suggestions for future experiments are presented, as well as conclusions based on the present analyses, in Sec. VI.

II. ANGULAR MOMENTUM DEPENDENT FISSION BARRIERS

The rotating liquid drop model⁷ predicts ground state and saddle point properties of nuclei as a function of a fissility parameter, x , and a rotational parameter, y , where

$$x = 0.0197(Z^2/A)/(1 - 1.783[(N - Z)/A]^2) \quad (1)$$

and

$$y = 1.93J^2/\{A^{7/3}(1 - 1.783[(N - Z)/A]^2)\} . \quad (2)$$

The x parameter is a measure of the ratio of the force of the disruptive Coulombic repulsion to the surface attractive force. The y parameter is related to the ratio of centrifugal repulsive force to surface attractive force. The fission barriers in the RLDM are the differences between ground state and saddle point energies as calculated in terms of the x and y parameters for idealized liquid drop nuclei (with sharp surfaces).

In Fig. 1 we show some nuclear shapes predicted by the RLDM as a function of the x and y parameters. The saddle point shapes can be described in terms of "compactness" (the ratio of the median semiminor axis to semimajor axis), and the "necking in," which refers to how small the cross sectional area of the neck is with respect to a cross sectional area of, e.g., a cylinderlike shape (as at $x=0.8$, $y=0$ in Fig. 1).

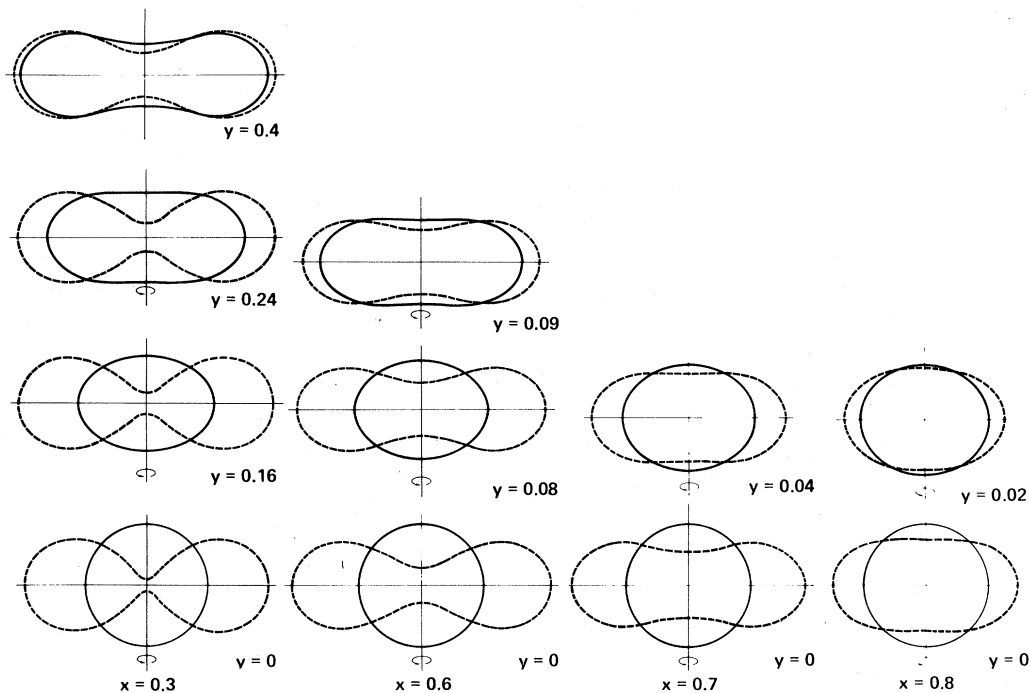


FIG. 1. Shape projections versus x (fissility) and y (angular momentum) parameters for the rotating liquid drop model. The dashed curves represent saddle point shapes and the solid curves represent equilibrium ground state shapes. The vertical axes are the axes of rotation. These shapes are based on the results of Ref. 7.

In Fig. 1, one observes an increase in compactness and a decrease in necking in with increasing x for the saddle point shapes. This implies decreasing fission barriers with increasing x . The effect of increasing angular momentum at fixed x is to make the saddle point more compact with less necking in. In this regard, the disruptive centrifugal parameter (y) acts qualitatively similar to the disruptive Coulomb parameter (x) in affecting saddle point properties.

The liquid drop model assumes nuclei of sharp surfaces. Krappe and Nix point out that the effect of the finite range of the attractive nuclear forces acting between two spheroids at the saddle point would tend to lower the saddle point energies with respect to a pure liquid drop prediction.⁸ Reference to Fig. 1 illustrates that qualitatively such a correction to the liquid drop barrier should decrease with increasing x , as predicted by Krappe and Nix (and later by Krappe, Sierk, and Nix).⁹ The barrier should also decrease with increasing y . This follows from the decrease in the surface areas of the two nascent fragments which are in close proximity at the saddle point. The effect due to the y parameter comes from two causes: a decrease in saddle point necking with an increase in y , and at quite high angular momenta where ground states have ceased to be oblate from the necking of the ground state shape which will tend to cancel the saddle point contribution. The latter statement follows simply from the fact that the fission barrier is the difference between the ground state and saddle point energies. As the two shapes approach each other (e.g., as y increases) the FR range corrections approach each other, and the effect on the barrier tends to vanish.

Several ways of calculating the FR correction versus the liquid drop model have been presented by Krappe *et al.*⁹ One is a direct comparison of predictions of the Yukawa-plus-exponential (FR) model⁹ with previously published LD parameters. These include an unrealistic radius parameter of 1.2249 fm in evaluation of Eqs. (1) and (2) (Ref. 7), as compared to an equivalent sharp radius parameter of around 1.16 fm from electron scattering. The second comparison made in Ref. 9 is with a renormalized LD model in which the radius parameter r_0 and surface asymmetry constant k_s are taken as 1.18 fm and 3.0, as used in the FR calculation. In this case the LD surface energy coefficient a_s was adjusted to give the same barrier for ^{236}U as in the Yukawa-plus-exponential (FR) model. The difference in barriers between these two sets of results versus Z^2/A is shown in Fig. 2. Both sets of LD

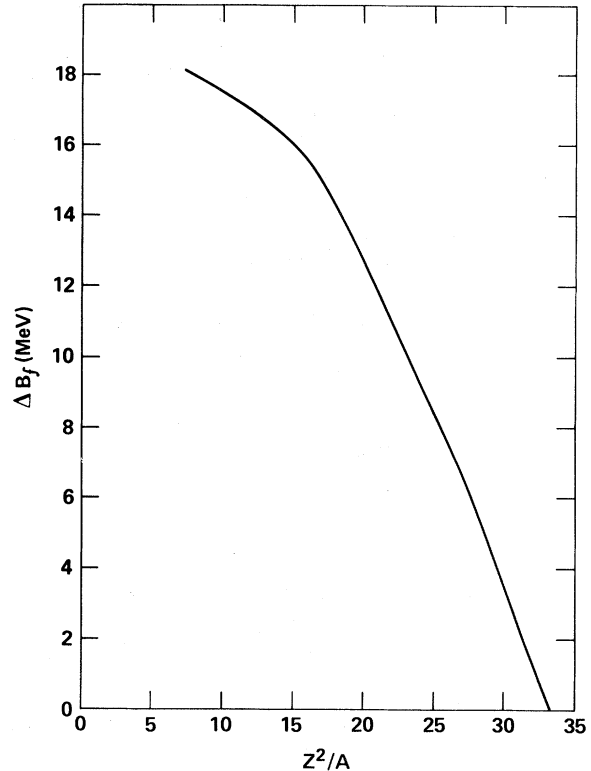


FIG. 2. Finite range correction prediction to the liquid drop barrier of nonrotating nuclei. This result is based on Fig. 12 of Ref. 9 (Krappe, Nix, and Sierk). The ordinate is the difference between barrier predictions with and without the finite range correction. The abscissa is the Z^2/A of the fissioning nucleus, calculated for β stable nuclei.

results will be considered later. The FR model gives a larger barrier decrement versus the modified LD model than versus the LD model with published constants ($r_0 = 1.2249$ fm). The validity of the renormalized LD model results is an open question, as it is based on a single barrier (^{236}U) and was not done globally. However, the *differences* between FR and the two sets of LD model barriers, which is of concern in this work, are approximately proportional; the modified LD result gives approximately twice the decrement versus FR model as is given by the unmodified LD model. Our final conclusions versus the modified LD barriers will, at worst, need modification by a proportionality constant.

It may be seen in Fig. 2 that very large corrections to the LD model are expected for lighter systems, and the effect is expected to disappear around $Z \sim 82$, $A \sim 200$. Comparisons with the cross sectional drawings of Fig. 1 are in qualitative agree-

ment with these comments; i.e., at $x=0$ (not shown) the saddle point configuration is given by two touching spheres, which would have the maximum FR correction; as x increases, the cross sectional area of the two fragments which are within a short range of one another may be seen to decrease, and as the neck between the nascent fragments disappears (around $x=0.8$) there should be no FR effect.

It is worthwhile to attempt to scale the angular

$$(Z^2/A)_{\text{eff tot}} = [(Z^2/A) + (L/L_{\text{ch}})^2] / [1 - 1.783((N-Z)/A)^2], \quad (3)$$

and with

$$L_{\text{ch}} = \frac{emr_0}{2^{5/3}f} A^{7/6}, \quad (4)$$

where A is the compound nucleus mass, e the electron charge, m the nucleon mass, r_0 the nuclear radius constant, and f the fraction of the angular momentum which is in the radial separation degree of freedom.¹¹ For symmetric fission we have used the value $f = \frac{5}{7}$. The quantity in the square bracket in the denominator of Eq. (3) is a symmetry correction, which is not included in $(Z^2/A)_{\text{eff tot}}$ defined in

momentum dependence due to the FR effect at least to first order. We attempt this, following the scaling method used by Swiatecki^{10,11} in his new dynamic fusion model, recognizing that the Coulombic and centrifugal forces are both disruptive in nature; the finite range correction might then be expected to be related to a total disruptive parameter $(Z^2/A)_{\text{eff tot}}$, which is the sum of the x and y contributions:

Refs. 10 and 11. If we use the finite range correction of Fig. 2 to correct RLDM fission barriers, replacing the (Z^2/A) of the abscissa with (3), we will refer to this as a "scaled FR barrier."

Angular momentum dependent barriers for three compound nuclei are shown in Fig. 3. The RLDM predictions are shown, as well as several adjusted barriers. The adjustments have been made by either subtracting a constant energy at every J , or by multiplying the barrier by a fixed fraction at each J . In the case of ^{97}Rh , the scaled FR barrier is also presented. It will be illustrated that any of the adjusted barriers shown permit a satisfactory reproduction of the experimental fusion/fission excitation functions.

It is obvious from Fig. 3 that the barrier parameters which fit fission results over some limited (high) angular momentum range all give different results when extrapolated to zero angular momentum. There is no justification in using any such curves for deducing values of fission barriers outside the range of sensitivity; in particular, the attempt to extrapolate to $J=0$ is totally arbitrary. The latter requires either light ion induced fission measurements (for which extremely low cross sections are expected), or at least proper theoretical modeling.

III. STATISTICAL MODEL FORMULATIONS

The statistical model codes used in the data analyses of the present work were of the Hauser-Feshbach type, including multiple particle emission and γ ray deexcitation. The code was a modification of the MBII code previously described. The equations governing particle emission and fission widths have been presented previously¹⁻³ and will not be repeated here. In this section, we describe the different options available and which have been used for treating level densities and transmission

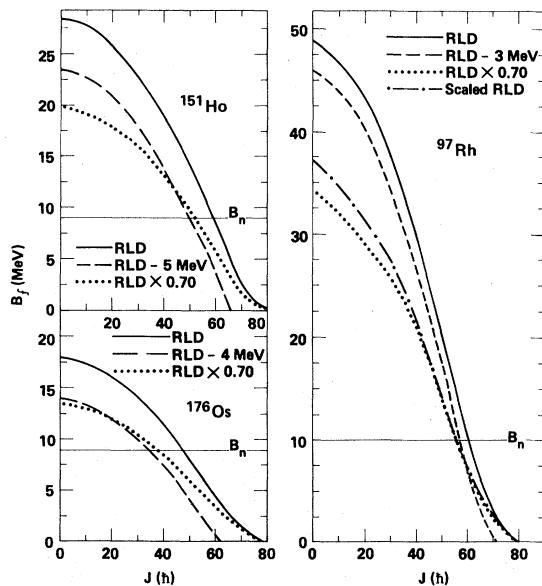


FIG. 3. Angular momentum dependent fission barriers for ^{97}Rh , ^{151}Ho , and ^{176}Os compound nuclei. The solid curves are RLDM predictions. Dotted curves represent RLDM barriers multiplied by 0.70 at all values of the angular momenta. The dashed curves represent RLDM results decremented by a constant energy at all values of the angular momenta. The dotted-dashed curve represents a scaling of the finite range correction using Eq. (3) to determine the abscissa.

coefficients within the context of the Hauser-Feshbach calculations.

A. Level density formulations

Several level density options were used in the present analyses. The basic form begins with the Fermi gas result,

$$\rho(E) = \frac{\sqrt{\pi}}{12} \frac{e^2 \sqrt{aE}}{a^{1/4} E^{5/4}}, \quad (5)$$

which is used to generate the angular momentum dependent level density^{12,13}

$$\begin{aligned} \rho(E, J) &= \frac{(2J+1)}{(8\pi)^{1/2} \sigma^3} \rho \left[E - \frac{J(J+1)\hbar^2}{2\mathcal{I}_{\text{rigid}}} \right] \\ &= \frac{(2J+1)}{(8\pi)^{1/2} \sigma^3} \rho(U), \end{aligned} \quad (6)$$

where $U = E - E_{\text{rot}}(J)$ and

$$E_{\text{rot}}(J) = \frac{J(J+1)\hbar^2}{2\mathcal{I}_{\text{rigid}}}$$

was taken from RLDM with

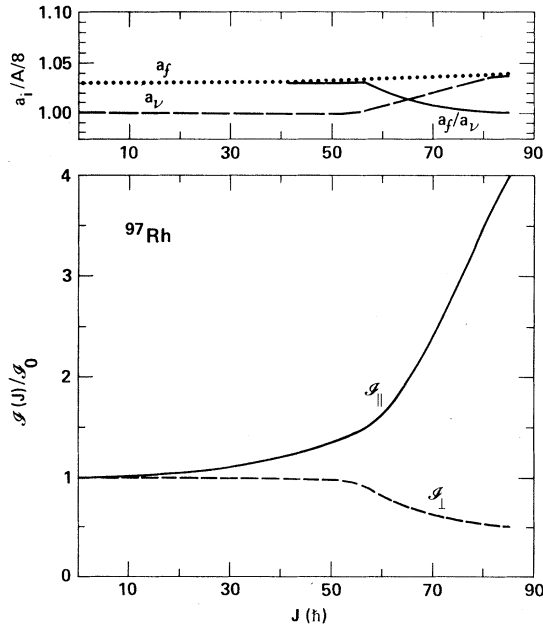


FIG. 4. Nuclear parameters versus angular momentum for ⁹⁷Rh. The upper portion shows a_f , a_v , and a_f/a_v as calculated from Eq. (11) versus angular momentum (J). The lower portion shows the ratio of moments of inertia parallel ($\mathcal{I}_{||}$) and perpendicular (\mathcal{I}_{\perp}) to the axis of rotation.

$$\sigma^3 = \left(\frac{\mathcal{I}_{\text{rigid}}}{\hbar^2} \right)^{3/2} \left(\frac{E}{a} \right)^{3/4}. \quad (7)$$

However, (6) has an implicit assumption of spherical symmetry. It has been pointed out that some collective enhancement (CE) of level densities should result for the nonspherical nuclei because of deformation due to angular momentum.^{14–17} The question has been left open as to the excitation energy at which CE ceases to be important. We will, therefore, analyze data using level density formulas with and without CE, to see the maximum uncertainty introduced into the fitting process due to the choice of level densities.

For nuclei with oblate deformation we have used the level density¹⁷

$$\begin{aligned} \rho(E, J) &= \frac{\hbar}{(8\pi\mathcal{I}_{||}\tau)^{1/2}} \\ &\times \sum_{K=-J}^J \rho \left[U - \frac{\hbar^2[J(J+1) - K^2]}{2\mathcal{I}_{\text{eff yrast}}} \right], \end{aligned} \quad (8)$$

where U is defined in Eq. (6), and for prolate nuclei (including saddle point nuclei)¹⁷

$$\rho(E, J) = \frac{\hbar}{(8\pi\mathcal{I}_{||}\tau)^{1/2}} \sum_{K=-I}^I \rho \left[U - \frac{\hbar^2 K^2}{2\mathcal{I}_{\text{eff}}} \right], \quad (9)$$

where $U = E - E_{\text{rot}}(J)$ as in Eq. (6) and

$$\mathcal{I}_{\text{eff}} = \mathcal{I}_{\perp} \mathcal{I}_{||} / (\mathcal{I}_{\perp} - \mathcal{I}_{||}), \quad (10)$$

with $\mathcal{I}_{\perp(\parallel)}$ representing the moment of inertia perpendicular (parallel) to the nuclear symmetry axis.

Relative values for parameters relevant to Eqs. (8)–(10) are summarized in Figs. 4 and 5. In Fig. 4 the ratios of $\mathcal{I}_{||}$ and \mathcal{I}_{\perp} to those for a spherical ⁹⁷Rh nucleus are shown versus J ; all calculated results are based on the RLDM. The effect of deformation on contributions to the level densities (7) and (8) are shown in Fig. 5 as contributions to the effective energies, and as these energies affect the level densities in the sum over K . The dotted curves in Fig. 5 indicate the $2J+1$ equally weighted orientations of the rotor in space when spherical symmetry applies. The dashed and solid curves represent the terms of Eqs. (8) and (9) when the less energetically favorable tumbling modes of a nonspherical rotor are considered. It may be seen that the prescriptions (8) and (9) have less than a $(2J+1)$ proportionality on angular momentum than the for-

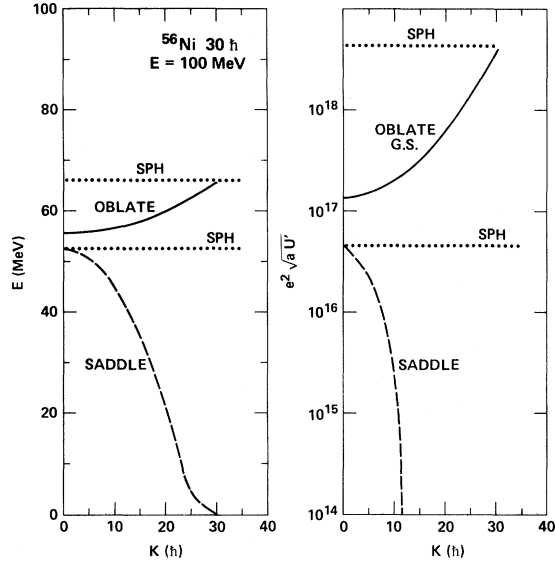


FIG. 5. Energies and exponential contributions to the sums of Eqs. (8) and (9) versus the value of K [Eqs. (8) and (9)] for ^{56}Ni . Results are presented for a nucleus excited to 100 MeV and $30\hbar$. The solid curves represent the ground state, which is predicted by RLDM to be oblate at $30\hbar$. The dashed curves represent the saddle point (prolate) configuration. The dotted curves represent contributions which would result if the nuclei were assumed to be spherical.

mulation for a spherically symmetric rotor (6). What this ultimately means in terms of barrier parameters extracted from the analyses to be performed can only be determined by doing the calculations.

B. Level density parameters

The level density parameters which are most crucial to the results of this work are the Fermi gas single particle level density parameters for the ground state (a_v) and saddle point nuclei (a_f). To first order, experiments are reproduced reasonably well by a value of $a_v \simeq A/8$, where A is the mass number of the daughter nucleus. Recent theoretical considerations are also in approximate agreement with this result.¹⁸ Accepting $a_v = A/8$ as a starting point, the value of a_f becomes a sensitive parameter in the fitting of fusion/fission excitation functions.

Because the saddle point is more highly deformed than the ground state, one expects (for a Fermi gas) that $a_f > a_v$ or $a_f/a_v > 1.0$. A simple model for predicting the dependence of the single particle level densities on deformation has been presented by Bishop *et al.*¹⁹ Their result may be expressed in terms of the ratio $\Delta_J = R_{\text{major}}/R_{\text{minor}}$ at angular

momentum J (where the R values refer to major and minor axes of the deformed nuclei) as

$$a_{v,f}(J) = \frac{A}{k} \frac{(33 + 4\Delta_J^{-2/3} + 2\Delta_J^{1/3})}{45}. \quad (11)$$

The value of k in Eq. (11) is the usual denominator for Fermi gas single particle parameters, $a = A/k$.

Many excitation functions have been analyzed with a_f/a_v taken as a free parameter (with $a_v = A/8$). The values extracted were generally within 1% of the results predicted by (11), with a 2% uncertainty.^{2,3} Therefore, the code used in this work has the option of calculating R_{major} and R_{minor} for every value of J based on RLD shapes; $a_f(J)$ and $a_v(J)$ are then computed independently at every value of the angular momentum, for each nuclide involved in the deexcitation process. In this work we have taken the value of k in Eq. (11) to be 8. The values of a_f and a_v are removed from the category of free parameters by this procedure, which has been used in the analyses of the present work. However, results will also be presented in which the $a_f(J)/a_v(J)$ ratios are varied by constant factors in order to verify that the *a priori* values given by (11) are within $\pm 1-2\%$ of the empirical "best" set. Some values of $a_f(J)$ and $a_v(J)$ calculated from Eq. (11) are shown in Fig. 4.

Binding energies used were based on the Myers and Swiatecki Lysekil mass parameters²⁰ including ground state shell corrections. Pairing corrections were based on $\delta = (11/A^{1/2})$ MeV (Ref. 20) with odd-even nuclei providing the reference point. Odd-odd nuclei were taken to have their thermodynamic excitation (E) plus δ MeV; even-even nuclei as $E - \delta$.

C. Transmission coefficients

The nuclei involved in fission deexcitation in heavy ion reactions often involved highly deformed ground state shapes. It has been shown that this may be expected to seriously alter the expected transmission coefficient distributions, which, in turn, can make large differences in fission/particle emission ratios.²¹⁻²³ It follows that any statistical fission parameters extracted from data analyses should depend upon the manner in which the transmission coefficients are modeled.

This question has been discussed in considerable detail in the literature. We have used previously reported algorithms based on RLDM shapes versus J with classical sharp cutoff model parametrizations in order to compute $T_l(E)$ for n , p , and α emission.^{22,23} In such a case the deformation was based

on the angular momentum J of the residual nucleus as described in Ref. 23. Results using $T_l^J(\epsilon)$ modeled in this fashion will be compared with results using $T_l(\epsilon)$ calculated assuming spherical nuclear shapes in order to illustrate the quantitative difference between the two approaches. For formulations of the algorithms used and comparisons with results using the nuclear optical model, we refer to Ref. 23. In the following text the notation $T_l^J(\epsilon)$ refers to transmission coefficients modeled for residual deformed nuclei and $T_l(\epsilon)$ refers to transmission coefficients calculated for spherical nuclei.

IV. COMPARISONS OF CALCULATED AND EXPERIMENTAL FUSION/FISSION EXCITATION FUNCTIONS

A. Systems selected and goals of analyses

Three main data sets plus several supplementary sets were selected for analyses in this work. These are summarized in Table I. The main sets were ^{35}Cl induced reactions on ^{62}Ni , ^{120}Sn , and ^{141}Pr targets.^{3,24-26} Results for these systems were measured over broader energy ranges than for any of the other systems. Additionally, both evaporation residue and fission angular distributions were measured at each energy used in the fitting procedures. Higher weighting will be given to these data sets in the final analyses.

We have included the data sets due to Plasil *et al.*⁴ ($^{12}\text{C} + ^{14}\text{Pr}$, $^{20}\text{Ne} + ^{133}\text{Cs}$) although we have serious reservations as to their accuracy regarding the maximum angular momentum for fusion. It has long been known that ^{12}C induced reactions, in particular, and reactions induced by ions of ^{20}Ne and lighter, undergo noncompound reactions with large cross sections at energies both near barrier and above.²⁷⁻³⁰ Even a 20% uncertainty in evaporation residue product yields would seriously alter the parameter set needed to fit these fission data. This point will be discussed further in Sec. V.

However, these data⁴ are potentially valuable (if the noncompound contributions could be accurately determined) because they include fission yields much lower than available in other data sets, thereby probing a different region of the angular momentum dependent fission barrier. This work represents an excellent experimental contribution of a difficult nature.

The question can be raised as to the uncertainties in analyses of the type to be presented which arise

TABLE I. Systems analyzed for fission parameters.

Proj.	Target	Com-pound	E_{lab} (MeV)	E^* (MeV)	$J_{\text{eff}}(\hbar)$
^{35}Cl	$+ ^{62}\text{Ni}$	$^{97}_{45}\text{Rh}$	155–300 ^a	86–179	60
^{40}Ca	$+ ^{60}\text{Ni}$	$^{100}_{48}\text{Cd}$	160–170 ^a	73–79	51
^{16}O	$+ ^{92}\text{Mo}$	$^{103}_{50}\text{Sn}$	187 ^b	149	60
^{12}C	$+ ^{141}\text{Pr}$	$^{153}_{65}\text{Tb}$	93–138 ^c	68–111	42
^{20}Ne	$+ ^{133}\text{Cs}$	$^{153}_{65}\text{Tb}$	103–129 ^c	64–88	40
^{35}Cl	$+ ^{116}\text{Sn}$	$^{151}_{67}\text{Ho}$	155–300 ^a	65–174	44
^{35}Cl	$+ ^{141}\text{Pr}$	$^{176}_{76}\text{Os}$	155–300 ^a	49–165	24
^6Li	$+ ^{197}\text{Au}$	$^{203}_{82}\text{Pb}$	75–95 ^d	81–101	35

^aB. Sikora *et al.* Phys. Rev. **20**, 2219 (1979); Phys. Rev. C **25**, 1446 (1982), and references therein.

^bS. Agarwal *et al.*, Z. Phys. A **296**, 287 (1980).

^cF. Plasil *et al.*, Phys. Rev. Lett. **45**, 333 (1980).

^dH. J. Karwowski, thesis, Indiana University Report 80-1 (1979); S. E. Vigdor, Nukleonika (to be published).

from nonequilibrium contributions to the fissionlike yields. This point has been explored in some depth in Ref. 3. The reader is referred to the latter for a full discussion of this point. The conclusion of that discussion is that if the evaporation yields are limited first by equilibrium fission competition, with nonequilibrium binary division mechanisms contributing at higher partial waves than the compound fission, then no error results in extracted statistical fission parameters due to nonequilibrium contributions to the fissionlike yields.

The data sets will be fitted first by modifying the RLD fission barriers by a constant decrement ΔB_f at all J , because this is the easiest method to understand in terms of RLD barrier modification. There is no theoretical justification for such an approach; therefore the absolute barrier heights extracted will be meaningful only over a narrow region of angular momenta over which the results are sensitive to the RLD barrier alteration. There is absolutely no justification for extrapolating such results either to higher or lower values of the angular momenta. We state again, in the absence of even a theoretical model prediction as to how to make an angular momentum dependent correction to RLDM barriers, any arbitrary method is *ad hoc*, and *at best* the parameters deduced are only valid over their limited range of sensitivity, and should not be extrapolated outside this range.

We will next show the sensitivity of fits to the form of level densities and choice of $T_l(\epsilon)$ or $T_l^J(\epsilon)$ for transmission coefficients. We will estimate the uncertainties in the ΔB_f correction terms due to the ambiguities in these quantities, as well as effects

due to changing the a_f/a_v ratios from the *a priori* values predicted by Eq. (11). These barrier decrements will be compared with predictions of the finite range model in Sec. V.

Additional analyses of data sets will be presented in which RLD barriers are all decreased by a constant factor k_f (as opposed to a constant energy ΔB_f as above). This will illustrate that alternative methods of parametrizing the barriers give almost equally satisfactory fits to the data. At the same time, the different methods of correction may give very different extrapolations to barriers at higher and/or lower J . This again emphasizes the dangers inherent in making such arbitrary extrapolations.

An *a priori* RLD barrier correction based on a scaled finite range correction (described in Sec. II) has been applied to the ^{97}Rh and ^{153}Tb excitation functions. This provides a crude theoretical modeling to an angular momentum dependent barrier correction, with an interesting result. Reasons for not treating heavier systems in this way will become clear in Sec. V.

B. Fits with constant barrier decrement

Figure 6 shows comparisons of calculated and experimental excitation functions for ^{97}Rh . Calculated results use RLD barriers with a 4 MeV decrement at all J ($\Delta B_f = 4$ MeV). Calculations were performed with transmission coefficients both for spherical and deformed nuclei; for each of these options level densities were used in the form for collective enhancement [Eqs. (8) and (9)] or for spherically rotors [Eq. (6)].

Figure 6 indicates that the lowest bombarding energy points (and therefore lowest J) are most sensitive to varying the choice of transmission coefficient or level density. Of the two choices, the use of $T_1^J(\epsilon)$ vs $T_1^J(\epsilon)$ results in roughly a factor of 3 change (decrease) in fission cross section, whereas the level density option yields a 33% decrease between the collective enhancement and spherical symmetry formulations. These statements pertain to the point at 155 MeV ^{35}Cl energy; the differences decrease with increasing excitation.

It is obvious in Fig. 6 that a 4 MeV decrement in $B_f(J)$ gives a satisfactory reproduction of the fission excitation function when $T_1^J(\epsilon)$ are modeled with consideration of nuclear deformation, and when level densities are computed with collective enhancement. But it is not clear that collective enhancement is called for at the relatively high excitation energies involved. What ΔB_f would be ap-

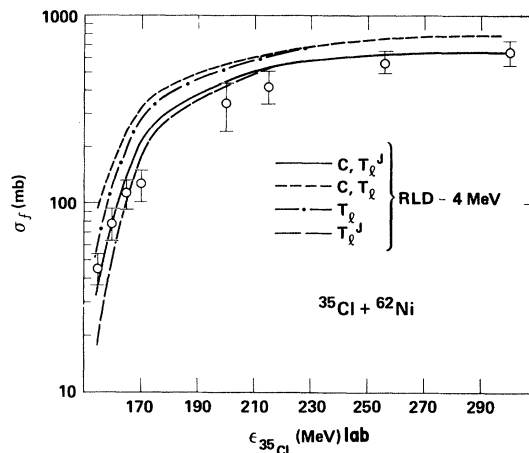


FIG. 6. Calculated and experimental fission excitation functions for the $^{35}\text{Cl} + ^{62}\text{Ni}$ reaction. All results are for RLD barriers which have been decremented by 4 MeV at every value of the angular momentum. The a_f and a_v values were from Eq. (11). Results are presented using level densities with collective enhancement as per Eqs. (8) and (9), indicated by "C" in the legend, and assuming spherical symmetry as per Eq. (6). Transmission coefficients were calculated for deformed nuclei (T_1^J) and assuming spherical nuclei (T_l). All deformed shapes were taken from the RLD predictions without modification.

propriate if collective enhancement is not used in the level density?

In Fig. 7, excitation functions are calculated with $\Delta B_f = 0$ and 2 MeV and compared with $\Delta B_f = 4$ MeV for a single choice of level density and transmission coefficients. At 155 MeV a 2 MeV

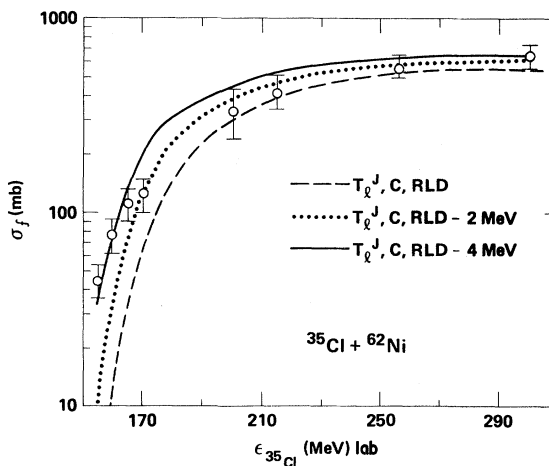


FIG. 7. As in Fig. 6, with level densities all for collective enhancement (C) and transmission coefficients all calculated for deformed nuclei. The RLD barriers have been decremented by 0, 2, and 4 MeV for the three sets of calculations presented.

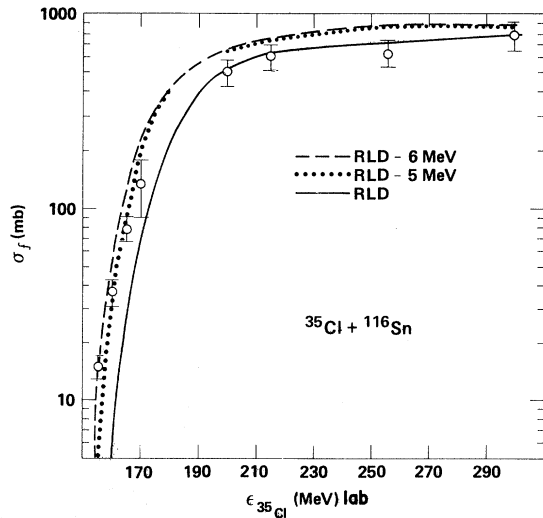


FIG. 8. Calculated and experimental excitation functions for $^{35}\text{Cl} + ^{116}\text{Sn}$. All level densities are for spherical nuclei, as are the T_l . The RLDM barriers were decremented by 0, 5, and 6 MeV.

change in ΔB_f results in roughly a factor of 4 change in σ_f . Therefore, we believe that the uncertainty of level density formulas between Eqs. (6) and (8) and (9) introduces at most an uncertainty of ± 1 MeV into the value deduced for ΔB_f . The difference, due to the choice of $T_l(\epsilon)$ or $T_l^J(\epsilon)$, is nearer to 1.5 MeV; however, we feel that the values for deformed nuclei are to be preferred on physical grounds. The uncertainty in ΔB_f due to level densi-

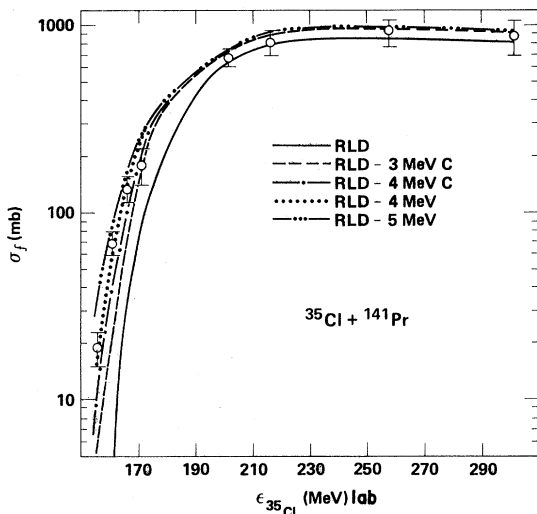


FIG. 9. Calculated and experimental fission excitation functions for $^{35}\text{Cl} + ^{141}\text{Pr}$. All T_l are for spherical nuclei. Level density choices and barrier decrements were according to the legends within the figure.

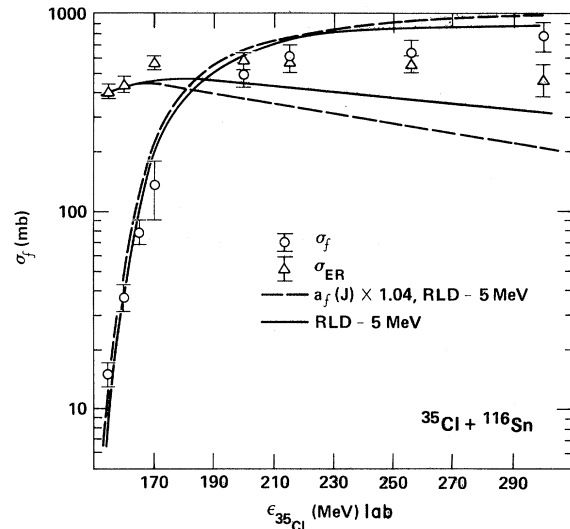


FIG. 10. Calculated and experimental fission and evaporation residue excitation functions for $^{35}\text{Cl} + ^{116}\text{Sn}$. The solid curves were calculated for a 5 MeV barrier decrement with $a_f(J)$ and $a_v(J)$ calculated with Eq. (11). The dashed curves have had the $a_f(J)$ of Eq. (11) multiplied by 1.04.

ty forms and choice of T_l decreases for higher mass systems.

Results for the ^{151}Ho and ^{176}Os compound systems are shown in Figs. 8 and 9. In Fig. 9, it may be seen that the use of CE level densities introduces an uncertainty of less than 1 MeV into ΔB_f . The effect of deformation on T_l is less because the ground state nuclei have very low deformations in the heavier nuclei in the region of J at which fission starts to become important.

C. Sensitivity of calculated excitation functions to a_f/a_v ratios

Figure 8 indicates that $\Delta B_f = 6$ MeV gives the best fit to the lowest energy fission cross section; $\Delta B_f = 5$ MeV fits most of the low energy fission cross sections. In Fig. 9, $\Delta B_f = 4$ MeV seems best. In Fig. 10, the ^{151}Ho fission and evaporation residue excitation functions have been calculated with $\Delta B_f = 5$ MeV, and with a_f multiplied by 1.04 over the values predicted by Eq. (11). Either result seems to reproduce the fission and evaporation residue (ER) cross sections at the lower bombarding energies satisfactorily. However, the $a_f(J) \times 1.04$ result may be seen to overestimate σ_f and seriously underestimate σ_{ER} at the higher bombarding energies. Consideration of the influences of a_f/a_v and ΔB_f effects on calculated results leads us to esti-

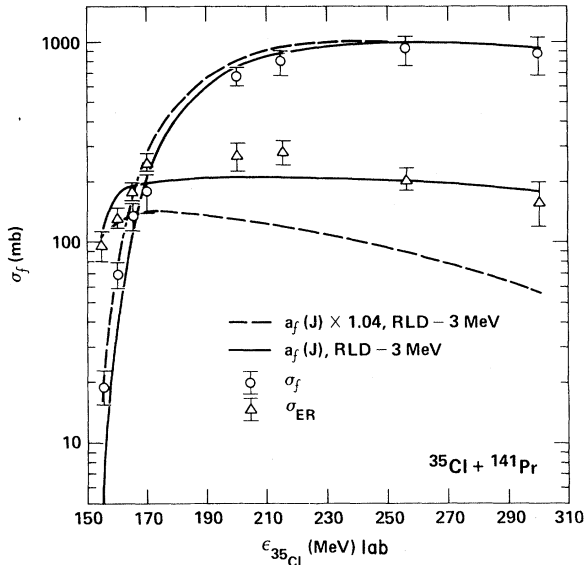


FIG. 11. As in Fig. 10 for the $^{35}\text{Cl} + ^{141}\text{Pr}$ reaction. The RLDM fission barriers were decremented by 3 MeV.

mate a $\Delta B_f = 5 \pm 1$ MeV for ^{151}Ho ; this result is sensitive around $J = 44\hbar$, and the uncertainty represents a reasonable range due to choice of a_f/a_v and level density formulations.

A similar comparison for ^{176}Os with $a_f(J) \times 1.04$ is shown in Fig. 11. This change in $a_f(J)$ brings the $\Delta B_f = 3$ MeV result of Fig. 9 into agreement with experiment at 155 MeV ^{35}Cl energy, but causes an underestimation of σ_{ER} by a factor of 3 at 300 MeV. It should be noted that when $\sigma_{\text{ER}} < \sigma_{\text{fission}}$, fitting the ER cross section is the more sensitive probe of a parameter set. Consideration of fits of the type shown in Figs. 9 and 11 leads us to estimate $\Delta B_f = 3 \pm 1$ MeV for the ^{176}Os nucleus. Similar fits were made for the other systems of Table I; results are summarized in Sec. V. The ^{153}Tb system is shown in Fig. 12 with calculated results for $\Delta B_f = 5$ MeV.

D. Proportional barrier reduction fitting

As previously discussed, the RLD barriers have often been parametrized by scaling by a constant multiplier to be determined by fitting experimental excitation functions,

$$B_f(J) = k_f \cdot B_f^{\text{RLD}}(J), \quad (12)$$

where $B_f^{\text{RLD}}(J)$ represents the fission barrier at angular momentum J predicted by the RLD model. Results of this type of fitting procedure may be seen

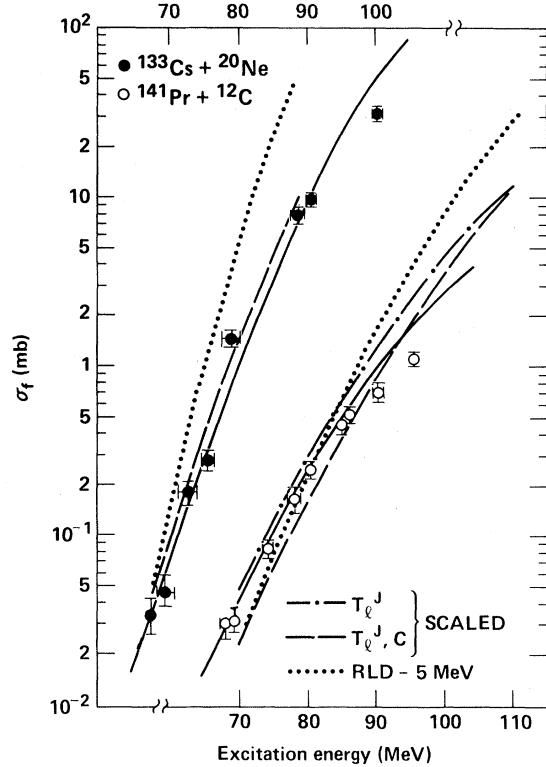


FIG. 12. Calculated and experimental fission excitation functions for the reactions $^{20}\text{Ne} + ^{133}\text{Cs}$ and $^{12}\text{C} + ^{141}\text{Pr}$. Experimental results are from Ref. 4. The dotted curve is for a constant RLDM barrier decrement of 5 MeV, T_l for spherical nuclei and level densities for spherical nuclei. The dashed and dotted-dashed curves were for RLDM fission barriers corrected for finite range effects at each J by scaling the result of Fig. 2 by the total disruptive parameter defined by Eq. (3).

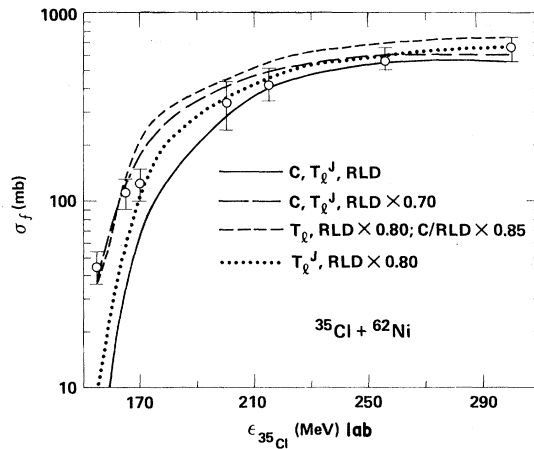


FIG. 13. $^{35}\text{Cl} + ^{62}\text{Ni}$ fission excitation function. Calculated results are for RLDM barriers scaled by a constant multiplier " k " at all angular momenta. The values used for " k " are indicated in the figure. Choice of level densities and transmission coefficients are also indicated.

in Figs. 13–15 for the ^{35}Cl induced reactions.

The values for ^{97}Rh reflect considerably less correction required for the RLD barriers than in analyses with the code MBII.³ This is mainly the result of separately computing level densities for every residual nuclide in the present code, as opposed to using the compound nucleus mass in the MBII code. Barrier reduction factors are also lower for the Ho and Os systems versus MBII results, but the differences are smaller.

Results of Figs. 13–15, if compared in the context of Fig. 3, would indicate similar barriers to those derived using ΔB_f corrections at the angular momenta at which fission is first measured. The use of different choices of level densities or T_l sets similarly requires no more than 1 MeV change in $B_f(J)$ over the appropriate range. We see that the fission excitation functions can be reproduced satisfactorily by two very different methods of modifying the RLDM barriers.

E. Scaled finite range barriers

In Sec. II we described a first order procedure by which the finite range result of Krappe, Sierk, and Nix for $J=0$ might be scaled for the influence of angular momentum.⁹ This would then remove the fission barrier height as a free parameter, just as the Bishop *et al.* prescription of Eq. (11) removes the a_f and a_v from the free parameter category.¹⁹ Results of such calculations are shown for ^{97}Rh in Fig. 16, and for ^{153}Tb in Fig. 12.

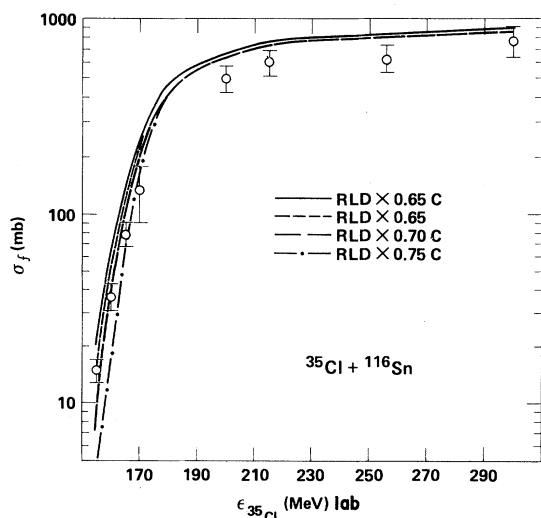


FIG. 14. $^{35}\text{Cl} + ^{116}\text{Sn}$ fission excitation function; as in Fig. 13.

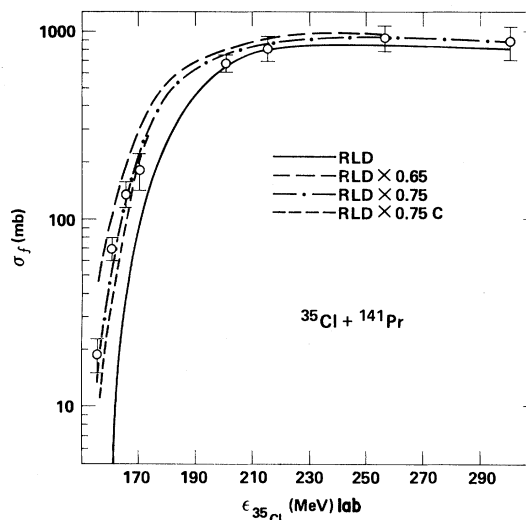


FIG. 15. $^{35}\text{Cl} + ^{141}\text{Pr}$ fission excitation function; as in Fig. 13.

Figure 16 shows excellent agreement with the entire fission excitation function for the calculation in which $T_l^J(\epsilon)$ were used with a level density with collective enhancement. The calculated result goes through every experimental point, giving a somewhat better overall agreement than the best result using a constant decrement correction to the RLD barriers. In general, the fit with a constant barrier multiplier (k_f) or a scaled barrier gives a better overall quality of fit than a barrier corrected via a constant decrement.

We note that the scaled barriers also give a some-

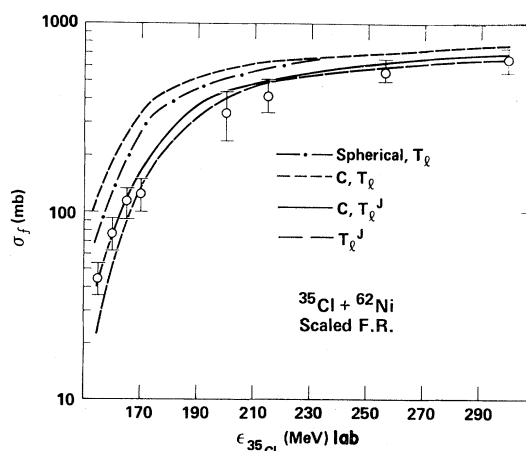


FIG. 16. $^{35}\text{Cl} + ^{62}\text{Ni}$ fission excitation function versus scaled finite range barrier correction calculations. Choices of level densities and transmission coefficients are as indicated. The RLDM barriers were scaled with angular momentum using the correction curve of Fig. 2 with the abscissa given by Eq. (3).

what better fit to the data in Fig. 12. However, we repeat our reservation that the magnitude of non-compound contributions observed for heavy ion reactions of $A \leq 20$ over the past two decades renders the data of Fig. 12 of questionable value for extraction of statistical fission parameters. In particular, if a part of the gross reaction product group which was identified in Ref. 4 as evaporation residues did, in fact, result from transfer reactions (e.g., ^8Be capture, α capture for ^{12}C induced reactions), then the $\Delta B_f = 5 \pm 1$ MeV deduced by fitting σ_f would increase in magnitude. The calculated results for the ^{20}Ne induced reaction stop at 88 MeV of excitation, since this was the highest energy at which experimental ER cross sections were reported (ER points were measured at three energies; of these the middle point was far outside reasonable errors and could not be used). The fits for $^{20}\text{Ne} + ^{133}\text{Cs}$ are therefore based on the $\simeq 65$ MeV and $\simeq 88$ MeV points; of these two points, neither the calculations of Ref. 4 nor the present results fit both points simultaneously (i.e., with a single parameter set).

V. COMPARISONS OF EXTRACTED ΔB_f WITH FINITE RANGE CORRECTION

The methods used in extracting ΔB_f corrections were described in Sec. IV A. Results are summarized in Table I, along with the angular momentum for which the fitting procedure begins (taken as l_{crit} for fusion for the lowest energy point fitted).

In Fig. 17, we show the finite range correction predicted by Krappe *et al.* for $Z^2/A > 20$. This is from Fig. 12 of Ref. 9 and represents the larger result of two different calculations. The calculated result is shown versus Z^2/A as calculated along the line of β stability but plotted with the asymmetry term correction of Eq. (3). On this curve we have plotted ΔB_f extracted as described in Sec. IV A (except that the result of Vigdor was used for the $^6\text{Li} + ^{197}\text{Au} = ^{203}\text{Pb}$ point without refitting, as his method of analysis was similar to ours). The points in Fig. 17 are plotted versus the Z^2/A of their compound nuclei, corrected for asymmetry according to Eq. (1).

It may be seen that there is no apparent correlation between the $J=0$ FR correction prediction and the ΔB_f results extracted from analyses of data. However, it was pointed out in Sec. II that the abscissa of Fig. 17 should be considered to be the ratio of *total* disruptive forces to surface attractive forces, rather than only the Coulomb disruptive force (which is the total at $J=0$).

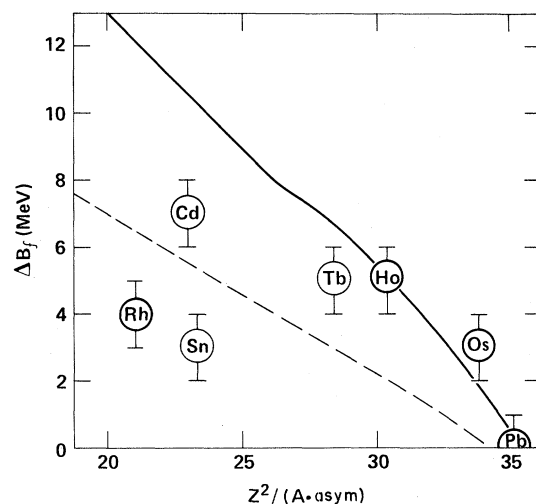


FIG. 17. Corrections deduced to RLDM barriers for various compound systems versus the Z^2/A of the compound systems. The systems analyzed are summarized in Table I, along with the angular momenta for which the deduced ΔB_f values are valid. The solid curve is the finite range correction prediction of Ref. 9 calculated for β stable nuclei. The heavier lined points represent systems having acceptably extensive evaporation residue and fission yield measurements, which should therefore give more reliable ΔB_f values. The dashed curve is the lower finite range correction prediction of Ref. 9. The abscissa has been corrected for symmetry as discussed in the text.

The ΔB_f points have therefore been replotted in Fig. 18, including the influence of the centrifugal force as per Eq. (3) to give an abscissa representing the total disruptive force. Here an immediate general agreement with the trend predicted by the FR

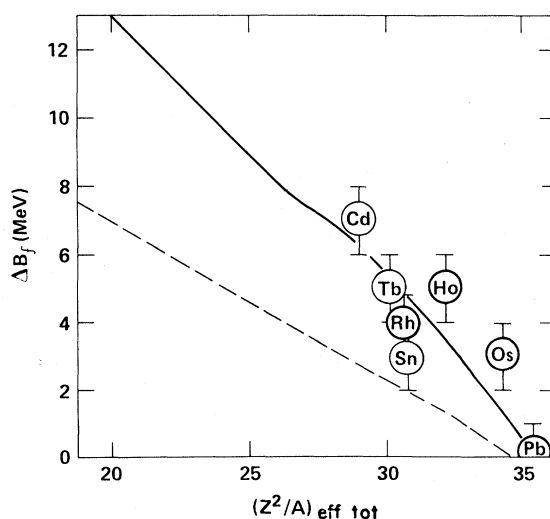


FIG. 18. As in Fig. 17, except that the experimental points have been replotted using Eq. (3) to calculate the abscissa. Solid and dashed curves are as in Fig. 17.

model may be seen.

If a "best FR correction" curve were to be drawn empirically through the ΔB_f points it would lie approximately 1.0 MeV above the result of Krappé *et al.*⁹ This statement would pertain only to the region $(Z^2/A)_{\text{eff tot}} \geq 29$, since we have no data points below this. While extrapolation is tempting, it is not justified. A constant correction of $\Delta B_f = 4$ MeV would almost fit these data points in Fig. 18 (with the exception of the ^{203}Pb point). It would clearly be desirable to have experimental values at lower values of $(Z^2/A)_{\text{eff tot}}$. Some data for α induced fission³¹ might be admissible for providing ΔB_f results at lower $(Z^2/A)_{\text{eff tot}}$ when analyses are performed with adequate consideration of precompound decay phenomena. Heavy ion reactions on lighter target systems, in which very low fission cross sections are measured (as was so nicely done in Ref. 4) may also provide the desired data.

The shift between data points and the FR curve in Fig. 18 is the reason that a scaled FR calculation (as in Fig. 16) would not work satisfactorily for the $^{35}\text{Cl} + ^{116}\text{Sn}$, ^{141}Pr systems; the data require a larger ΔB_f at the lower angular momenta than is indicated by the FR curve predicted in Ref. 9 and used in our code. If a curve roughly 1 MeV higher than the solid curve of Fig. 18 were used in the computer code rather than the solid curve, the scaled FR calculation would be expected to give a good reproduction of all the data on which we place a high weighting. (The ^{97}Rh excitation function would show good agreement at energies from 170 MeV and above.)

VI. SUMMARY AND CONCLUSIONS

We have illustrated that, beginning with the RLD as a reference source for computing J dependent fission barriers, there are any number of different ways in which the barriers might be systematically modified versus angular momentum in order to reproduce experimental fusion/fission excitation functions. Of the methods employed, the use of a constant decrement is the simplest to interpret in terms of the modification required of the RLD barriers in the region of angular momentum at which fission starts to be observed. These results may be compared with predictions of the FR correction; if the abscissa includes centrifugal force for the experimentally extracted ΔB_f , a qualitative agreement is found with the FR prediction. A shift upward of the FR correction curve ≈ 1 MeV is suggested by the empirically deduced ΔB_f results (for

$Z^2/A > 29$). We also agree with earlier conclusions that the a_f and a_v parameters may be satisfactorily predicted by the formula of Bishop *et al.*, where shell effects are not of overriding importance in determining fission barriers ($A \leq 200$).^{2,3,6}

The only calculation we have presented in which the fission barriers are modified based on modeling (rather than empirically scaling them) is what we have called the "scaled FR" method. This worked well for the ^{97}Rh system but would fail for the heavier systems due to the (~ 1 MeV) upward shift suggested by the data over FR predictions. Such an uncertainty is, of course, well within the order of shell effects which have been predicted to persist at higher angular momenta for certain nuclei³²; whether such shell effects persist to the relatively high excitations of the present work is doubtful. Nonetheless this suggests analyses of the type provided in Fig. 18 over a much broader data set would be desirable. The narrow range of $(Z^2/A)_{\text{eff total}}$ covered by the experimental results points out the desirability of experiments selected to probe lower $(Z^2/A)_{\text{eff total}}$ ranges. The centrifugal contribution must not be overlooked when selecting the experimental system.

If suggestions for additional experiments are clear, so too are the roads necessary in theory. The *ad hoc* scaling of the FR correction must be replaced by a proper calculation for the rotating drop in which the finite range effect is included as well as the effect of surface diffuseness (which will modify the moment of inertia of the rotating system). Such calculations are underway by several groups.^{33,34} It will be of interest to see if the shift implied by the points in Fig. 18 might be explicable in terms of uncertainties in the mass parameters.

Finally we observe that some works purporting to analyze heavy ion data for fission barrier information have concluded that there are basic disagreements between different works. We see no cause for such a conclusion based on the data which we have analyzed to date, when the analyses and comparisons are made with basic considerations of the physics involved, and when the inherent uncertainties in such analyses are included. We are optimistic that proper choice of experiments and careful analyses, coupled with nuclear modeling, will permit a mapping of the angular momentum dependent fission barriers to quite reasonable accuracy.

This work was performed under the auspices of the U.S. Department of Energy by the Lawrence Livermore National Laboratory under Contract No. W-7405-ENG-48.

- ¹J. R. Huizenga, R. Chaudhry, and R. Vandenbosch, *Phys. Rev.* **126**, 210 (1962).
- ²H. Freiesleben, H. C. Britt, and J. R. Huizenga, *Proceedings of the Third International Atomic Energy Symposium on Physics and Chemistry of Fission* (IAEA, Vienna, 1974), Vol. I., p. 447; see also Refs. 1–4 therein.
- ³M. Beckerman and M. Blann, *Phys. Lett.* **68B**, 31 (1977); *Phys. Rev. C* **17**, 1615 (1978); B. Sikora, W. Scobel, M. Beckerman, and M. Blann, *Phys. Rev. C* **25**, 1446 (1982).
- ⁴F. Plasil *et al.*, *Phys. Rev. Lett.* **45**, 333 (1980).
- ⁵W. von Oertzen *et al.*, *Z. Phys. A* **298**, 207 (1980).
- ⁶S. E. Vigdor, *Nukleonika* (to be published); see also H. Karwowski, IUCF Internal Report No. 80-1, 1979.
- ⁷S. Cohen, F. Plasil, and W. J. Swiatecki, *Ann. Phys. (N.Y.)* **82**, 557 (1974).
- ⁸H. J. Krappe and J. R. Nix, *Proceedings of the Third International Atomic Energy Symposium on Physics and Chemistry of Fission* (IAEA, Vienna, 1974), Vol. I, p. 159.
- ⁹H. J. Krappe, J. R. Nix, and A. J. Sierk, *Phys. Rev.* **20**, 992 (1979).
- ¹⁰W. J. Swiatecki, *Phys. Scr.* **24**, 113 (1981).
- ¹¹W. J. Swiatecki, *Nucl. Phys.* **A376**, 275 (1982).
- ¹²T. Ericson, *Adv. Phys.* **9**, 425 (1960).
- ¹³D. W. Lang, *Nucl. Phys.* **77**, 545 (1966).
- ¹⁴T. Ericson, *Nucl. Phys.* **6**, 62 (1958).
- ¹⁵J. R. Huizenga *et al.*, *Nucl. Phys.* **A223**, 589 (1974).
- ¹⁶S. Bjornholm, A. Bohr, and B. R. Mottelson, *Proceedings of the Third International Atomic Energy Symposium on Physics and Chemistry of Fission* (IAEA, Vienna, 1974), Vol. I, p. 373.
- ¹⁷L. G. Moretto, see Ref. 16, p. 329.
- ¹⁸J. Toke and W. J. Swiatecki, *Nucl. Phys.* **A372**, 141 (1981).
- ¹⁹C. J. Bishop, I. Halpern, R. W. Shaw, Jr., and R. Vandenbosch, *Nucl. Phys.* **A193**, 161 (1972).
- ²⁰W. D. Meyers and W. J. Swiatecki, *Ark. Fys.* **36**, 343 (1967).
- ²¹M. Blann, *Phys. Lett.* **88B**, 5 (1979).
- ²²M. Blann, *Phys. Rev. C* **21**, 1770 (1980).
- ²³M. Blann and T. A. Komoto, *Phys. Rev. C* **24**, 426 (1981).
- ²⁴J. Bisplinghoff *et al.*, *Phys. Rev. C* **17**, 177 (1978).
- ²⁵P. David *et al.*, *Nucl. Phys.* **A287**, 179 (1977).
- ²⁶B. Sikora *et al.*, *Phys. Rev. C* **25**, 686 (1982).
- ²⁷R. Bimbot, D. Gardes, and M. F. Rivet, *Nucl. Phys.* **A189**, 193 (1972).
- ²⁸K. Siwek-Wilczynska *et al.*, *Phys. Rev. Lett.* **42**, 1599 (1979).
- ²⁹P. D. Croft and J. M. Alexander, *Phys. Rev.* **165**, 1380 (1968).
- ³⁰K. A. Geoffroy *et al.*, *Phys. Rev. Lett.* **43**, 1303 (1979).
- ³¹L. G. Moretto, S. G. Thompson, J. Routh, and R. C. Gatti, *Phys. Lett.* **38B**, 471 (1972); G. M. Raisbeck and J. W. Cobble, *Phys. Rev.* **153**, 1270 (1967).
- ³²M. E. Faber and M. Ploszajczak, *Phys. Scr.* **24**, 189 (1981).
- ³³M. G. Mustafa and C. D. Castro, *Bull. Am. Phys. Soc.* **26**, 1120 (1981); M. G. Mustafa, P. A. Baisden, and H. Chandro, *Phys. Rev. C* **25**, 2524 (1982).
- ³⁴A. J. Sierk, private communication.